



Glioblastoma adaptation traced through decline of an IDH1 clonal driver and macro-evolution of a double-minute chromosome

Favero, Francesco; McGranahan, Nicholas; Salm, Maximilian P.; Birkbak, Nicolai Juul; Sanborn, J. Zachary ; Benz, Stephen C. ; Becq, Jennifer; Peden, John F. ; Kingsbury, Zoya ; Grocok, Russell J.

Total number of authors:

11

Published in:

Annals of Oncology

Link to article, DOI:

[10.1093/annonc/mdv127](https://doi.org/10.1093/annonc/mdv127)

Publication date:

2015

Document Version

Publisher's PDF, also known as Version of record

[Link back to DTU Orbit](#)

Citation (APA):

Favero, F., McGranahan, N., Salm, M. P., Birkbak, N. J., Sanborn, J. Z., Benz, S. C., Becq, J., Peden, J. F., Kingsbury, Z., Grocok, R. J., & Eklund, A. C. (2015). Glioblastoma adaptation traced through decline of an IDH1 clonal driver and macro-evolution of a double-minute chromosome. *Annals of Oncology*, 26(5), 880-887. <https://doi.org/10.1093/annonc/mdv127>

General rights

Copyright and moral rights for the publications made accessible in the public portal are retained by the authors and/or other copyright owners and it is a condition of accessing publications that users recognise and abide by the legal requirements associated with these rights.

- Users may download and print one copy of any publication from the public portal for the purpose of private study or research.
- You may not further distribute the material or use it for any profit-making activity or commercial gain
- You may freely distribute the URL identifying the publication in the public portal

If you believe that this document breaches copyright please contact us providing details, and we will remove access to the work immediately and investigate your claim.

Glioblastoma adaptation traced through decline of an IDH1 clonal driver and macroevolution of a double minute chromosome

Francesco Favero^{1,2,*}, Nicholas McGranahan^{1,3,*}, Maximilian Salm^{1,*}, Nicolai J. Birkbak^{1,4,*}, J. Zachary Sanborn⁵, Stephen C. Benz⁵, Jennifer Becq⁶, John F. Peden⁶, Zoya Kingsbury⁶, Russell J. Grocock⁶, Sean Humphray⁶, David Bentley⁶, Bradley Spencer-Dene¹, Alice Gutteridge⁴, Michael Brada^{7,8}, Stupp Roger⁹, Pierre-Yves Dietrich¹⁰, Tim Forsheew⁴, Marco Gerlinger^{1,11}, Andrew Rowan¹, Gordon Stamp¹, Aron C. Eklund², Zoltan Szallasi^{2,12,13}, Charles Swanton^{1,4}

¹Cancer Research UK London Research Institute, London, United Kingdom

²Center for Biological Sequence Analysis, Department of Systems Biology, Technical University of Denmark, Lyngby, Denmark

³Centre for Mathematics & Physics in the Life Sciences & Experimental Biology (CoMPLEX), University College London, London, United Kingdom

⁴University College London Cancer Institute, London, United Kingdom

⁵NantOmics, LLC, Santa Cruz, CA, USA

⁶Illumina Ltd, Cambridge, United Kingdom

⁷Department of Molecular and Clinical Cancer Medicine, University of Liverpool, Liverpool, United Kingdom

⁸Department of Radiation Oncology, Clatterbridge Cancer Centre NHS Foundation Trust, Bebington, United Kingdom

⁹Department of Oncology, University Hospital Zurich, Zürich, Switzerland

¹⁰Centre of Oncology, University Hospitals of Geneva, Switzerland

¹¹Centre for Evolution and Cancer, The Institute of Cancer Research, London, United Kingdom

¹²Children's Hospital Informatics Program at the Harvard-MIT Division of Health Sciences and Technology (CHIP@HST), Harvard Medical School, Boston, MA, USA

¹³MTA-SE NAP, Brain Metastasis Research Group, Hungarian Academy of Sciences, 2nd Department of Pathology, Semmelweis University, Budapest 1091

© The Author 2015. Published by Oxford University Press on behalf of the European Society for Medical Oncology.

This is an Open Access article distributed under the terms of the Creative Commons Attribution Non-Commercial License (<http://creativecommons.org/licenses/by-nc/4.0/>), which permits non-commercial re-use, distribution, and reproduction in any medium, provided the original work is properly cited. For commercial re-use, please contact journals.permissions@oup.com

Correspondence to: Prof. Charles Swanton, Cancer Research UK London Research Institute, 44 Lincoln's Inn Fields, London, WC2A 3LY, United Kingdom. Phone: (+44) 207 269 3463; Fax: (+44) 207 269 3094; charles.swanton@cancer.org.uk

*Contributed equally

Abstract:

Background

Glioblastoma (GBM) is the most common malignant brain cancer occurring in adults, and is associated with dismal outcome and few therapeutic options. GBM has been shown to predominantly disrupt three core pathways through somatic aberrations, rendering it ideal for precision medicine approaches.

Methods

We describe a 35 year-old female patient with recurrent GBM following surgical removal of the primary tumor, adjuvant treatment with temozolomide, and a 3-year disease-free period. Rapid whole genome sequencing (WGS) of three separate tumour regions at recurrence was performed and interpreted relative to WGS of two regions of the primary tumour.

Results

We found extensive mutational and copy number heterogeneity within the primary tumour. We identified a *TP53* mutation and two focal amplifications involving *PDGFRA*, *KIT* and *CDK4*, on chromosomes 4 and 12. A clonal *IDH1* R132H mutation in the primary, a known GBM driver event, was detectable at only very low frequency in the recurrent tumour. After subclonal diversification, evidence was found for a whole genome-doubling event and a translocation between the amplified regions of *PDGFRA*, *KIT* and *CDK4*, encoded within a double minute chromosome also incorporating miR26a-2. The WGS analysis uncovered progressive evolution of the double minute chromosome converging on the *KIT/PDGFRA/PI3K/mTOR* axis, superseding the *IDH1* mutation in dominance in a mutually exclusive manner at recurrence, consequently the patient was treated with imatinib. Despite rapid sequencing and cancer-genome

guided therapy against amplified oncogenes, the disease progressed, and the patient died shortly after.

Conclusions

This case sheds light on the dynamic evolution of a GBM tumor, defining the origins of the lethal subclone, the macroevolutionary genomic events dominating the disease at recurrence and the loss of a clonal driver. Even in the era of rapid WGS analysis, cases such as this illustrate the significant hurdles for precision medicine success.

Keywords:

Glioblastoma, multiregion sequencing, intratumour heterogeneity, double minute

Key Message: "In a glioblastoma tumour with multiregion sequencing before and after recurrence, we find an IDH1 mutation that is clonal in the primary but lost at recurrence. We also describe the evolution of a double minute chromosome encoding regulators of the PI3K signaling axis that dominates at recurrence, highlighting the challenges of an evolving and dynamic oncogenic landscape for precision medicine."

Introduction

Glioblastoma (GBM) is the most common malignant brain cancer occurring in adults and is associated with poor prognosis and a median overall survival of only 15 months[1]. Nearly all GBM tumours recur after surgery, radiotherapy and chemotherapy, with a median time to recurrence of 7 months[1].

Accumulating evidence suggests that treatment failure in cancer may be driven by intratumour heterogeneity (ITH) and branched tumour evolution involving genetically distinct subclones[2]. Recent studies have documented widespread ITH in GBM. Sottoriva et al[3] found that each individual tumour can harbour multiple distinct copy-number profiles and transcriptomic subtypes simultaneously. Johnson et al[2] revealed spatial and temporal heterogeneity in GBM, confirmed the importance of *TP53* and *IDH1* as early driver mutations[4, 5], and demonstrated the impact of temozolomide (TMZ) treatment on tumour evolution, with 6 of 10 tumours showing evidence of TMZ-induced hypermutation at recurrence.

In order to fully assess ITH within the life-history of a single tumour and attempt to offer the patient a cancer genome-guided therapy, we implemented rapid multi-region whole-genome sequencing (WGS) in a patient with recurrent GBM. This analysis reveals the temporal and spatial evolution of a GBM tumour, defining the origins of the lethal subclone from a subclone in the primary tumour and the associated macroevolutionary genomic events dominating the disease at recurrence, confounding treatment success.

Methods

Ethics

Written informed consent was obtained from the patient in the Hospitaux Universitaires de Geneve “Analyse de la reponse immunologique contre les tumeurs cerebrales” translational approved protocol IRB 03-126. Tumour material was analysed under the UCL-Cancer Institute and Pathology biobank (UCLHRTB 10/H1306/42). The patient provided written informed consent to tumour sequencing analysis within a compassionate setting. The study was

conducted according to the provisions of the Declaration of Helsinki and the Good Clinical Practice Guidelines of the International Conference on Harmonization.

WGS data processing and analysis

WGS was performed by Illumina, UK. **Mutation calling** and filtering was performed using VarScan2 as described [6], annotation of coding mutations were performed using ANNOVAR[7]. **Structural variant (SV)** breakpoint mechanism classification was performed according to the criteria defined in Yang et al[8]. Reconstruction of the putative double minute chromosomes was performed as described in Sanborn et al[9] and breakpoints mapping to the focal amplifications were validated by PCR and Sanger Sequencing. **Copy number variation (CNV)** analysis was performed on the WGS data. Purity, ploidy and allele-specific copy number estimates were obtained with Sequenza [10]. **Clonal analysis** was performed as described in Bolli et al [11], estimating the cancer cell fraction (CCF) by integrating variant allele frequency estimates with copy number, purity and ploidy estimates. Single sample and multi-sample Dirichlet process clustering was performed using the DPpackage R package[12]. In this work, mutations are referred to as “subclonal” if their CCF indicates they are present in only a subset of cancer cells within a given sample ($CCF < 1$). Mutations present in all cancer cells of a given sample ($CCF = 1$) are referred to as “clonal”. **Genome doubling** was determined from the comparison of the sequencing of the grade II and the grade IV regions and by considering the mutations located in the portion of the genome where a clear doubling of the number of alleles was detected, see Supplementary Information for details. All data analysis was performed in R version 3.0.2, all p-values are two-sided.

Results

Clinical case report

A 35-year-old female presented with partial complex seizures in January 2007, increasing in frequency after the delivery of her second child in September 2007 (Figure 1A). MRI carried out in June 2008, revealed a right temporal mass (6x6.7x4.5 cm) with slight contrast enhancement. She underwent complete

removal of the tumour on July 3rd, 2008 and the diagnosis of WHO grade IV astrocytoma (GBM) was established (the tumour consisted of a grade II and grade IV histological components). She received concomitant treatment with irradiation (60 Gy in 30 fractions) and TMZ, followed by 6 monthly cycles of TMZ (200 mg/m² D1-D5) until March 2009. She was free of symptoms for two years but partial seizures reappeared in early 2011. A further MRI showed a multifocal recurrence in the right temporal area extending to the thalamus and the corpus callosum. Considering the long disease free interval (3 years) between first treatment and recurrence, TMZ at a similar dose and schedule was prescribed again.

In March 2012, she presented with acute headache and intracranial hypertension. MRI showed massive progression mainly in the right frontal area with risk of herniation. She underwent partial removal of the tumour on March 29th, 2012. The histology confirmed grade IV astrocytoma with *MGMT* gene promoter methylation. She received bevacizumab and TMZ; after transient clinical improvement, her clinical condition deteriorated and TMZ was replaced by 800mg imatinib daily, guided by the WGS data, sequenced and reported within 7 days by Illumina, indicating amplification of *KIT* and *PDGFRA*. The tumour progressed rapidly on therapy and she died 3 months after the 2nd surgical debulking procedure.

Whole genome sequencing

Archival formalin fixed paraffin embedded (FFPE) specimens of the grade II and IV primary samples along with three fresh-frozen samples from the recurrence and a germline reference were WGS to a depth of 30X ($\sim 1.3 \times 10^6$ paired reads per sample; Table S1 in Supplementary Information). The three recurrence regions were homogeneous at the SNV level indicating limited clonal variation in the recurrence, however the SNV calling was hampered by stromal contamination (Table S1). The 3 recurrent regions, referred to as A1, A2 and A3, respectively, were merged *in silico* in a single alignment file, termed As, to increase the resolution and improve the capacity to define the evolutionary trajectory of the recurrence specimen. 1271 and 1935 high-confidence somatic

silent and non-silent SNVs were identified in the grade II and IV regions respectively, and 1435 in the recurrence specimen. When comparing the grade II and grade IV to the recurrence, the grade IV shared 338 mutations with the recurrence not found in the grade II region, while the grade II only shared 1 mutation with the recurrence not found in the grade IV region (Figure 1B, coding mutations only in Figure S1, detailed mutation information in Supplementary File). Given that the grade II region exhibited fewer private mutations (69/1271, Figure 1B, 1C), this indicates it most closely resembles the most recent common ancestor (MRCA), and that the recurrence specimen evolved from the grade IV region.

Extensive mutational variation found between grade II and grade IV regions

Several clonal mutations were found in both primary lesions suggesting a shared clonal origin. These include a *TP53* Y220C mutation, a frame shift mutation in *ATRX* (K1871fs), and an *IDH1* mutation, R132H. These genes have previously been described as driver events for GBM[4, 13], and *ATRX* mutations has been shown to co-occur with *TP53* and *IDH1* mutations [2], and to be a driver of alternative telomere lengthening[14]. Clustering the mutation CCFs in the grade II grade IV regions revealed six distinct clusters (Figure 1D). Most mutations were identified as clonal in both primary lesions or as clonal in one but missing from the other (clusters 1, 3 and 6). However, we also found 202 mutations that were clonal in the grade IV but subclonal in the grade II (cluster 2), and two clusters of mutations (4 and 5) that were subclonal in the grade IV and absent in the grade II. The cluster 2 mutations likely represent a persistent subclone within the grade II region that gave rise to the grade IV region, while clusters 4 and 5 may have arisen independently in the grade IV, consistent with further subclonal evolution occurring during disease progression.

Primary tumour shows heterogeneous acquisition of copy number changes

CNV and SV analyses identified a number of shared events in the primary regions (Supplementary Table S2), including copy-neutral loss of heterozygosity (LOH) on chromosome 17p following *TP53* mutation (Figure S2 A-B); *CDK6* and *MET*

amplification via gain of 7q; and two high level focal amplifications (Figure S3) of 4q12 (encoding *PDGFRA* and *KIT*) and 12q13.3-q14.1 (encoding *CDK4*, *AVIL* and miR-26a-2).

ITH was also detected by CNV and SV analyses (Figure S4): *CDKN2A/B* loss and other CNVs (gain of 6p, 19p and 20p; loss of 10q, 12q, 13, 16q, 17q and 22) were detected only in the grade IV sample. Furthermore, the 4q12 and 12q13.3-14.1 focal amplifications were linked by numerous translocations in the grade IV but not in the grade II sample (Figure S5, Figure S6).

Allele-specific CNV analysis revealed that the grade IV region was predominantly tetraploid, while the grade II region was largely diploid. Mutations in the grade IV region also exhibited a bimodal variant allele frequency distribution consistent with a genome-doubling (GD) event, exclusively in the grade IV region (Figure S7). As previously reported [15], GD is permissive for chromosome instability (CIN) and accelerated cancer genome evolution. Consistent with a GD event in the grade IV region followed by chromosome losses due to increasing CIN[15], flow cytometry on the fresh tissue of the three recurrence samples, revealed a DNA-index of 1.60, 1.58 and 1.55 for each recurrence region (Figure S8).

Chromosome 4 rearrangements and evolution of a double minute chromosome

Copy-number analysis of the recurrence tumour revealed focal amplifications in 4q12 and 12q13.3-q14.1 detected in the grade IV region, with comparably high copy number and seemingly identical breakpoints (Figure S2C-D, Figure S6). Although the grade II sample also shared the 12q13.3-q14.1 amplification, the entire 4q-arm was amplified in this sample. Structural variant analysis revealed complex chromosomal re-arrangements linking the 4q12 and 12q13.3-q14.1 focal amplifications in the higher-grade samples only. Taken together, these features are reminiscent of a double minute chromosome, a relatively frequent cytogenetic event in GBM[9, 16].

To investigate this further, we employed a precise amplicon reconstruction method[9]. This involved the identification of breakpoints related to the highly amplified regions, followed by the construction of a breakpoint graph that links the amplified segments and their associated breakpoints, and a final search for an optimal path that completely traverses the graph (Figure S9). In the final solution, segment traversal number correlates with observed relative copy-number of the segment, and circular paths are indicative of a double minute chromosome.

Consistent with a double minute chromosome, the 4q12 and 12q13.3-q14.1 amplifications revealed circular paths, indicating double minute chromosomes in the grade IV and recurrence samples (Figure 2A-B & S9A). Two chromosomal intervals (Figure 2A) replete with putative driver genes (*PDGFRA*, *KIT*, *CDK4*, *AVIL* and *miR-26a-2*) are re-configured into circular assemblies. Figure 2B illustrates the optimal paths that account for the observed breakpoints and high copy-number amplifications. The absence of this structure in the grade II sample suggests that the 12q13.3-q14.1 focal amplification preceded DM formation, consistent with a breakage-bridge fusion cycle[17]. However, L1 elements flank the 12q13.3-q14.1 amplification (data not shown), precluding further local SV resolution. There are numerous precisely shared breakpoints between the double minute models, and all breakpoints tested validated (Figure 2C & S10), which suggests a common origin of the extra-chromosomal structures. Moreover, the breakpoints exhibit features of non-homologous end-joining[8] which may be indicative of a single chromothriptic event[18].

To investigate the origin of the DMs, we performed haplotype analysis in the grade IV and recurrence DMs. This was achieved using allele frequencies of heterozygous SNPs located in the DM locus (Supplementary Information). Consistent with a shared origin of the DMs, the allelic composition of the DM haplotypes appears to be identical at the 4q12 and 12q13.3-q14.1 loci (Figure S11). Moreover, the DM derived from both higher copy-number haplotypes; conversely, the higher copy-number haplotypes on 4q12 were predominantly lost in the segments flanking the DM. Such a pattern is consistent with shattering

of a “gained” chromosome 4q followed by “rescue” of oncogenic fragments within the DM and loss of the remainder of the chromosome.

Double-minute chromosome is associated with progression

We computed a distance matrix from all the mutations detected in the primary regions and in the three recurrence regions, establishing a phylogenetic relationship between the sequenced regions. This confirmed that the recurrence specimen was most similar to the grade IV region, with the DM likely arising between the grade II and grade IV regions (Figure 3A). The DM carries the putative GBM driver gene *AVIL*[19], with a mutation restricted to the grade IV/recurrence lineage and linked to the focal amplification via discordant paired-end reads as well as exhibiting a high variant allele frequency (chr12:58204830; Figure S2F). Additionally, the DM unifies multiple oncogenic components of the PI3K pathway: *PDGFRA*, *KIT*, and a regulator of *PTEN* (miR-26a-2) as well as *CDK4* (Figure 2B). To assess if the grade IV tumour shows increased activation of the PI3K pathway, we performed immunohistochemistry against PDGFRA, PTEN and cKIT in the grade II and grade IV tumours (Figure 3B). We found increased levels of PDGFRA (215/300 versus 93/300, grade IV versus grade II) and cKIT (222/300 versus 31/300) in the grade IV tumour, but no difference in the PTEN levels (34/300 versus 23/300). This suggests that PTEN is deactivated in both the grade II and grade IV tumours, but that the PI3K pathway is further activated in the grade IV tumour, likely due to amplification of genes encoded within the double minute chromosome.

IDH1 driver mutation is lost at recurrence

Trunk events including the *TP53* and *ATRX* mutations and *PDGFRA/KIT*, *CDK4/miR-26a-2* focal amplifications along with the grade IV private mutation detected in *AVIL* were identified at high frequency in the recurrence samples. Surprisingly, the *IDH1* R132H mutation was not detected in the recurrence samples despite being clonal in the grade II and IV lesions. To validate this observation, we performed digital PCR (dPCR) on *IDH1* and *TP53* (using *TP53* as a control). We confirmed that the R132H mutation was indeed clonal in the grade II and grade IV specimens (found in approximately 42-44% of DNA molecules, Supplementary File), but essentially undetected in the recurrence

samples, with between 0.01% and 0.1% of DNA molecules showing the mutation by dPCR. Conversely, *TP53* was found in between 8% and 12% of the DNA molecules (Supplementary File), consistent with clonal presence in the low-purity recurrence biopsies (estimated at 10-15% purity, Supplementary Information). It is likely therefore that the recurrence has experienced loss of the mutated *IDH1* allele and retention of the wild-type allele.

A recent report indicates mutual exclusivity between activation of the PI3K pathway and IDH1 activity[20]. As the recurrence demonstrated increased levels of *PDGFRA* and *KIT* amplification encoded on the DM, activators of the PI3K pathway, we addressed whether the GBM data from The Cancer Genome Atlas (TCGA)[16] supports mutual exclusivity between *IDH1* R132H mutation and *PDGFRA* and/or *KIT* amplification. *IDH1* and *TP53* mutations are enriched in the proneural subtype[21]. Using the cBio portal[22], we identified 137 TCGA GBM cases classified as proneural in Brennan et al [16], with both sequence and copy number data. Of these, 12 showed the R132H mutation, 25 showed dual *KIT* and *PDGFRA* amplification, and 10 showed *PDGFRA* amplification only. No overlap between cases with the *IDH1* R132H mutation and *KIT* and/or *PDGFRA* amplification was detected, indicating mutual exclusivity between these oncogenic events ($P=0.036$, Fisher's exact test). This also suggests that the *IDH1* R132H mutation was indeed an early driver event that was subsequently lost during recurrence, as a more potent polyoncogene-oncomir cluster was selected for in the DM.

An analysis of TCGA GBM data from 264 tumours with whole exome sequencing processed by Sanborn et al[9] to infer DM structures, identified four samples, of these three proneural, with amplifications of both *PDGFRA* and *CDK4*, possibly encoded in double minute chromosomes. These data suggest that at least 1.5% (4/264) of GBM tumours overall, and 8% (22/264) of the proneural subtype, are driven by the acquisition of such a macro-evolutionary event typified by *PDGRA/CDK4/miR-26a-2* DMs.

Discussion

This study is the first report of a multi-region longitudinal WGS of a glioblastoma from diagnosis to death, performed specifically with the intention to improve patient outcome by the application of tailored therapy. Unfortunately, despite identifying multiple amplified targetable oncogenes and applying targeted therapy, disease control was not achieved, and the patient died following disease progression.

To our knowledge, this is the first description of a loss of a tier 1 clonal driver event (*IDH1*, R132H) during disease progression, and may reflect complex epistatic relationships between tumour somatic events and the selection pressure of therapy. While it is formally possible that the recurrence evolved from a subclone lacking the *IDH1* mutation, this would require extensive parallel evolution since the majority of somatic aberrations were shared between relapse and the grade IV region. Rather, the progressive enrichment of the DMs from the grade IV to recurrence suggests increased oncogenic potential based on the PI3K pathway. With the waning of the driver *IDH1* event this indicates a macro-evolutionary switch from the dominance of the *IDH1*-mutated tumour to a DM-driven tumour in a mutually exclusive context. An analysis of the TCGA data also revealed no overlap between *IDH1* R132H mutations and *PDGFRA/KIT* amplification, suggesting that high level *PDGFRA/KIT* amplification would not be favourable with an existent *IDH1* R132H mutation.

These findings have important implications for precision medicine, suggesting a targetable clonal driver event can be selectively lost during the disease course, and replaced in its entirety by an initially low frequency event in the primary tumour. The clonal dominance of *IDH1* driver events might need to be considered within the context of low frequency oncogenic drivers when examining the efficacy of therapeutics targeting *IDH1* in this disease[23]. Furthermore, despite rapid WGS at recurrence and cancer genome-directed therapy, imatinib was unable to control the disease. Following radiotherapy and two surgical debulking procedures, it is unlikely that the blood-brain barrier was intact, preventing drug penetration into the central nervous system. It is more

likely that treatment failure was a consequence of the evolution of the poly-oncogene/oncomir DM targeting the PI3K axis at multiple nodal points.

Moreover, our results highlight the profound effects of cancer cell genome doubling, resulting in accelerated cancer genome evolution, characterized by a tolerance of CIN and propagation of aneuploid progeny [15]. The accelerated CIN permitted following the genome doubling event in the grade IV region of the primary tumour, and possibly a chromothripsis event on chromosome 4, resulted in the formation and subsequent selection of a highly polyoncogene-oncomir DM encoding *miR-26a-2*, *PDGFRA*, *KIT* and *CDK4*.

MicroRNA *miR-26a-2* effectively targets PTEN[24]. Immunohistochemistry demonstrated that PTEN expression was weak or absent relative to stromal cells in both the grade II and grade IV regions, although no genomic aberrations were detected at the *PTEN* locus. It is likely therefore, that amplification of *CDK4/miR-26a-2* region, either encoded within the DM in the grade IV region and recurrent tumour or simply due to amplification as observed in the grade II specimen, directly contributed to loss of PTEN protein expression.

Taken together, these observations emphasise the complexity of signal transduction cascades activated within individual tumours. However, it is apparent that the oncogenic drivers involved in GBM pathogenesis are highly constrained and the combination of these events involved in DMs may be finite. There is an unmet need to enroll patients within longitudinal cohort studies to define these genetic constraints in order to accelerate our understanding of GBM evolution throughout the disease course and optimise therapeutic opportunities in this disease.

Acknowledgments:

Results published here are partially based upon data generated by the Cancer Genome Atlas pilot project established by the NCI and NHGRI. Information about TCGA and the investigators and institutions who constitute the TCGA research

network can be found at <http://cancergenome.nih.gov/>. The data were retrieved through dbGaP authorization (Accession No. phs000178.v8.p7).

Funding:

This work was supported by the European Commission 7th Framework Programme [HEALTH-2010-F2-259303]; Z.S was funded by The Breast Cancer Research Foundation, the Hungarian Academy of Sciences (KTIA_NAP_13-2014-0021).

Disclosure:

JB, JFP, ZK, RJG, SH and DB are employees of Illumina Inc, a public company that develops and markets systems for genetic analysis. The remaining authors declare no competing financial interests.

Reference:

1. Wen PY, Kesari S. Malignant gliomas in adults. *N. Engl. J. Med.* 2008; 359(5):492–507.
2. Johnson BE, Mazar T, Hong C et al. Mutational analysis reveals the origin and therapy-driven evolution of recurrent glioma. *Science* 2014; 343(6167):189–93.
3. Sottoriva A, Spiteri I, Piccirillo SGM et al. Intratumor heterogeneity in human glioblastoma reflects cancer evolutionary dynamics. *Proc. Natl. Acad. Sci. U. S. A.* 2013; 110(10):4009–14.
4. Watanabe T, Nobusawa S, Kleihues P, Ohgaki H. IDH1 mutations are early events in the development of astrocytomas and oligodendrogliomas. *Am. J. Pathol.* 2009; 174(4):1149–53.
5. Turcan S, Rohle D, Goenka A et al. IDH1 mutation is sufficient to establish the glioma hypermethylator phenotype. *Nature* 2012; 483(7390):479–83.
6. De Bruin EC, McGranahan N, Mitter R et al. Spatial and temporal diversity in genomic instability processes defines lung cancer evolution. *Science* (80-.). 2014; 346(6206):251–256.
7. Wang K, Li M, Hakonarson H. ANNOVAR: functional annotation of genetic variants from high-throughput sequencing data. *Nucleic Acids Res.* 2010; 38(16):e164.
8. Yang L, Luquette LJ, Gehlenborg N et al. Diverse mechanisms of somatic structural variations in human cancer genomes. *Cell* 2013; 153(4):919–29.

9. Sanborn JZ, Salama SR, Grifford M et al. Double minute chromosomes in glioblastoma multiforme are revealed by precise reconstruction of oncogenic amplicons. *Cancer Res.* 2013; 73(19):6036–45.
10. Favero F, Joshi T, Marquard AM et al. Sequenza: allele-specific copy number and mutation profiles from tumor sequencing data. *Ann. Oncol.* 2014:mdu479–.
11. Bolli N, Avet-Loiseau H, Wedge DC et al. Heterogeneity of genomic evolution and mutational profiles in multiple myeloma. *Nat. Commun.* 2014; 5:2997.
12. Jara A, Hanson TE, Quintana FA et al. DPpackage: Bayesian Non- and Semi-parametric Modelling in R. *J. Stat. Softw.* 2011; 40(5):1–30.
13. Liu X-Y, Gerges N, Korshunov A et al. Frequent ATRX mutations and loss of expression in adult diffuse astrocytic tumors carrying IDH1/IDH2 and TP53 mutations. *Acta Neuropathol.* 2012; 124(5):615–25.
14. Lovejoy CA, Li W, Reisenweber S et al. Loss of ATRX, genome instability, and an altered DNA damage response are hallmarks of the alternative lengthening of telomeres pathway. *PLoS Genet.* 2012; 8(7):e1002772.
15. Dewhurst SM, McGranahan N, Burrell RA et al. Tolerance of whole-genome doubling propagates chromosomal instability and accelerates cancer genome evolution. *Cancer Discov.* 2014; 4(2):175–85.
16. Brennan CW, Verhaak RGW, McKenna A et al. The somatic genomic landscape of glioblastoma. *Cell* 2013; 155(2):462–77.
17. Bunting SF, Nussenzweig A. End-joining, translocations and cancer. *Nat. Rev. Cancer* 2013; 13(7):443–54.
18. Forment J V, Kaidi A, Jackson SP. Chromothripsis and cancer: causes and consequences of chromosome shattering. *Nat. Rev. Cancer* 2012; 12(10):663–70.
19. Crespo I, Tão H, Nieto AB et al. Amplified and homozygously deleted genes in glioblastoma: impact on gene expression levels. *PLoS One* 2012; 7(9):e46088.
20. Charitou P, Rodriguez-colman M, Gerrits J et al. FOXOs support the metabolic requirements of normal and tumor cells by promoting IDH 1 expression. *EMBO Rep.* 2015; Epub ahead(Feb 3):1–11.
21. Verhaak RGW, Hoadley KA, Purdom E et al. Integrated genomic analysis identifies clinically relevant subtypes of glioblastoma characterized by abnormalities in PDGFRA, IDH1, EGFR, and NF1. *Cancer Cell* 2010; 17(1):98–110.
22. cBioPortal for Cancer Genomics. [<http://www.cbioportal.org/public-portal/>].

23. Yap TA, Gerlinger M, Futreal PA et al. Intratumor heterogeneity: seeing the wood for the trees. *Sci. Transl. Med.* 2012; 4(127):127ps10.
24. Lee DH, Amanat S, Goff C et al. Overexpression of miR-26a-2 in human liposarcoma is correlated with poor patient survival. *Oncogenesis* 2013; 2:e47.

FIGURES LEGENDS

Figure 1: Timeline and clonal structure.

Timeline of the patient's disease from diagnosis to death (**A**) timing for the temozolomide (TMZ), bevacizumab (BEV) and imatinib treatments. Timeline is not drawn to scale in terms of length of time.

A Euler-Venn diagram (**B**) displaying the overlaps of non-silent and silent mutations in the joint recurrence cohort and the grade II and grade IV samples. A mutation spectrum of non-synonymous mutations is illustrated as an heatmap of the detected mutations in the 2 primary tumour sectors and in the joint 3 recurrence samples (**C**). Squares coloured in yellow represent mutations detected in sub-clonal populations in the specific sector while red squares represent the presence of the mutation in the clonal population of the respective sector.

(**D**) Two-dimensional clustering of mutations in the grade II and grade IV specimens. The axis correspond the cancer cell fraction (CCF), describing the fraction of tumour cells carrying the mutation. The ordinate corresponds to grade IV specimen and the abscissa corresponds to grade II specimen. Clusters present on the upper right of the plot correspond to clonal mutations present in both specimen; clusters located in the upper left represent clonal mutations unique of the grade IV and the bottom right correspond to clonal mutations unique of the grade II specimen.

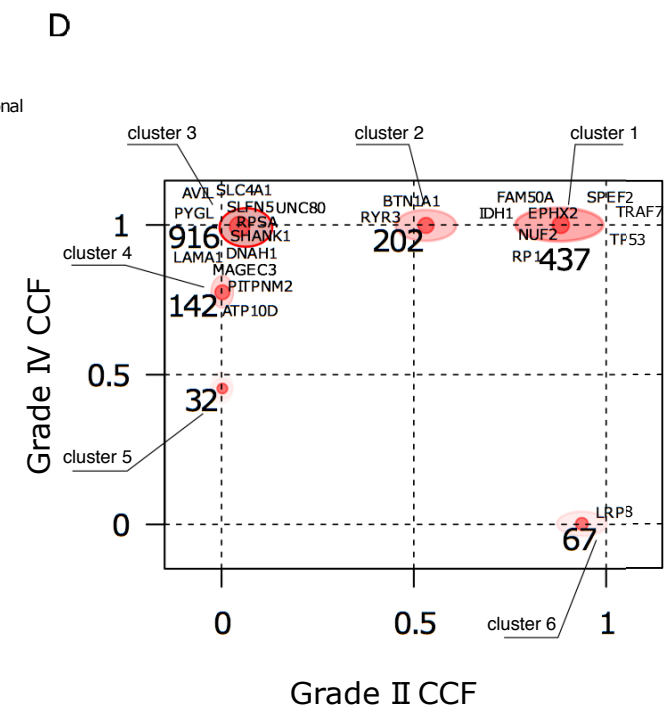
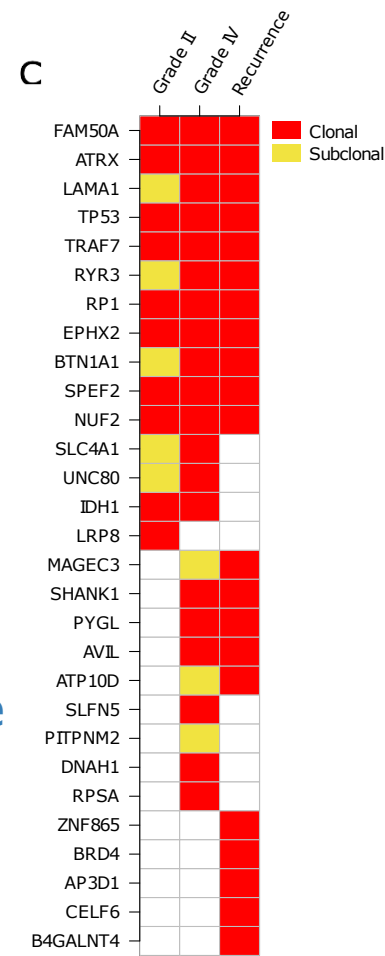
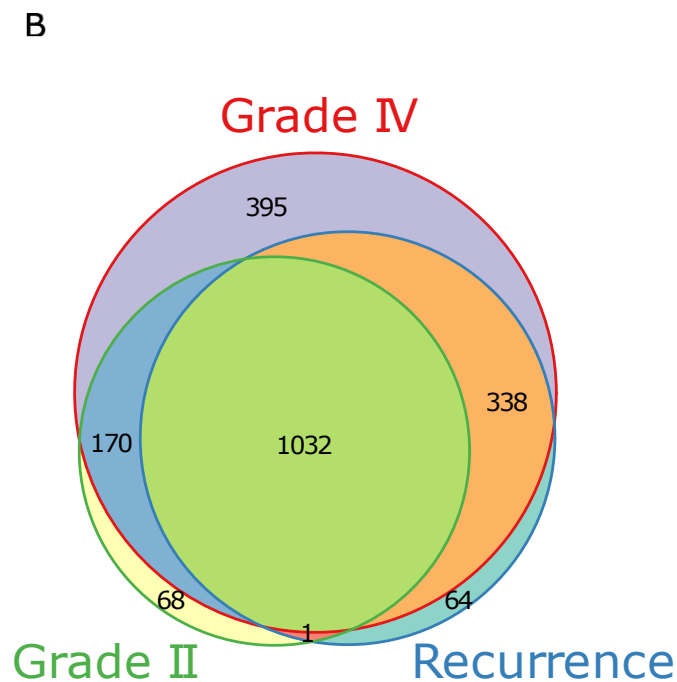
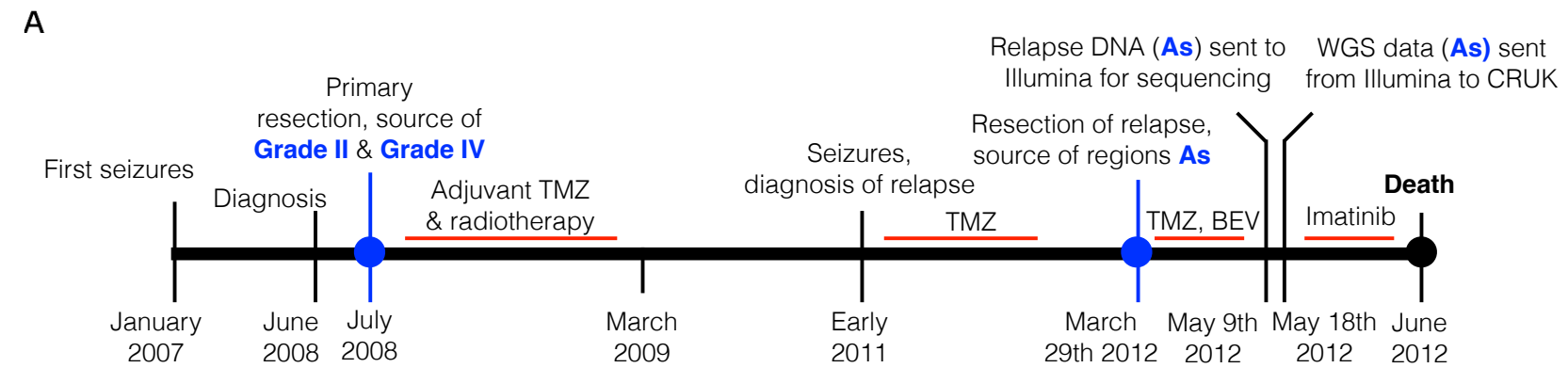
The numbers close to each cluster represent the number of non-silent and mutations present in the respective cluster, gene symbols represent non-synonymous mutation present in the cluster.

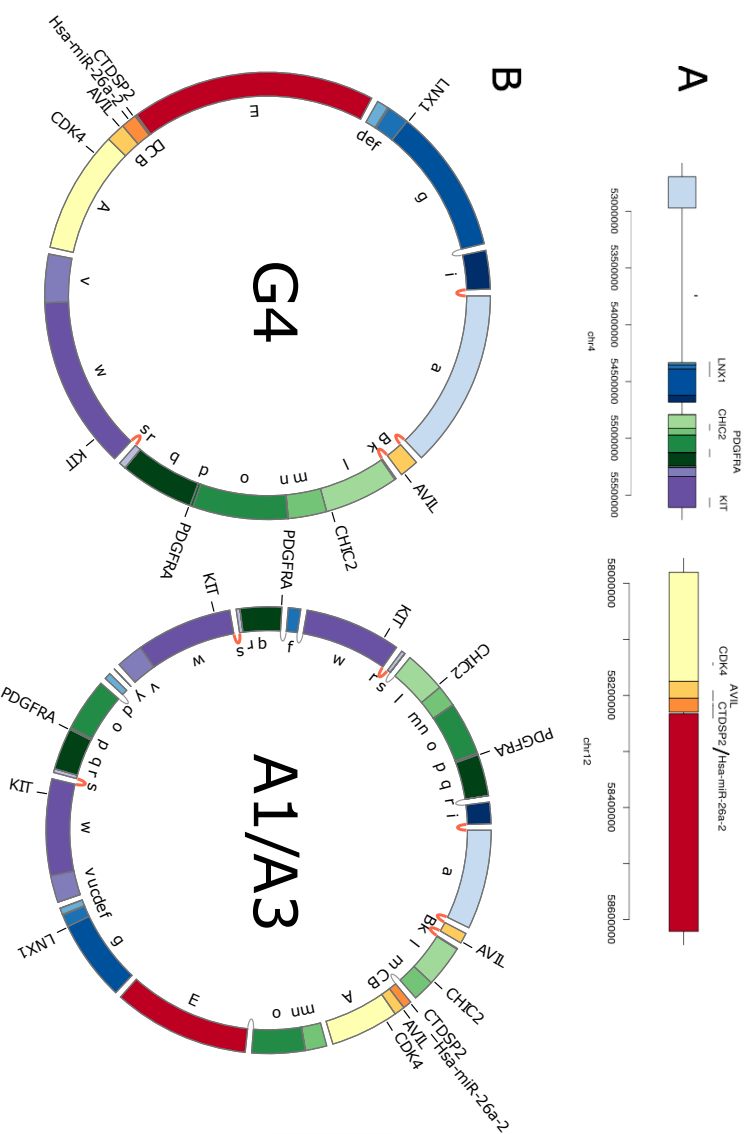
Figure 2: Evolution of the double minute

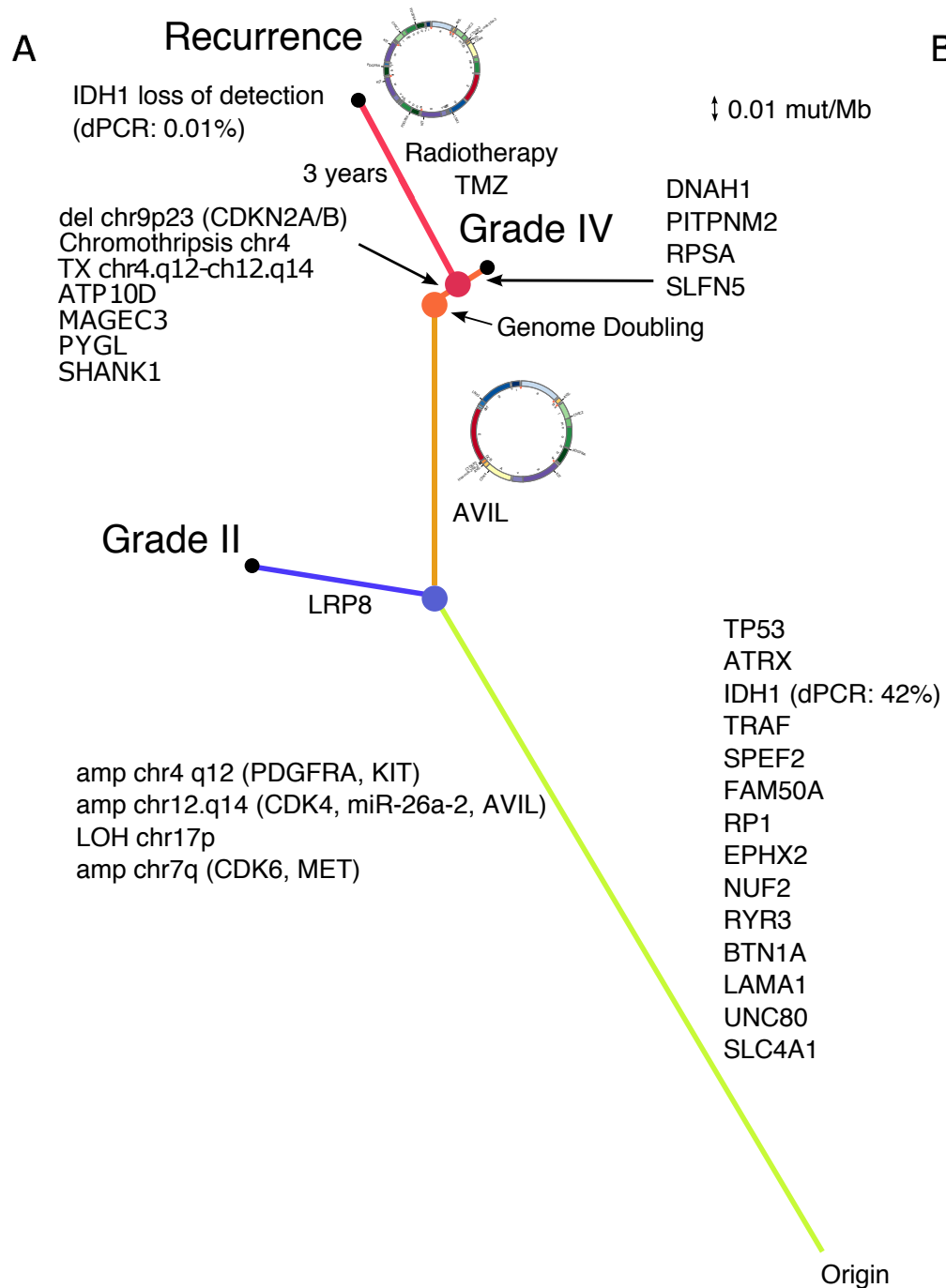
(A) The upper panel represents the genomic segments prior to the DM formation, with genes annotated by horizontal lines. The lower panel contains circular chromosome plots representing the double-minute models for the grade IV (**G4**) and recurrence samples (**A1/A3**), with validated (and shared) breakpoints denoted by red links between segments. Light grey links represent un-validated breakpoints for which *de novo* contigs could be assembled. Validated breakpoints are illustrated in panels **B** and **C**

Figure 3 Evolution a GBM tumor to recurrence

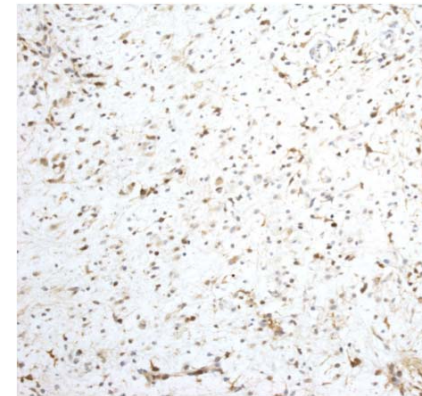
(A) Phylogenetic tree describing the evolution of the tumour. The length of the branches is calculated using the mutation rate as described in the method section. The recurrence specimens are characterised by loss of the *IDH1* mutation and by the further evolution of the double minute. Blue dot represents branching of Grade II and Grade IV specimens, orange dot represents the genome-doubling event, red dot represents branching of recurrence tumour from the Grade IV specimen. Black dots represent tumour sampling. For *IDH1*, mutant allele frequency detected by dPCR is indicated in parenthesis (**B**) Immunohistochemistry showing increased expression of *cKIT* and *PDGFRA* in the grade IV component of the primary tumour relative to grade II. *PTEN* is highly expressed in the proliferating vessels of both the grade II and IV primary tumour sectors but the neoplastic astrocytes are largely negative.



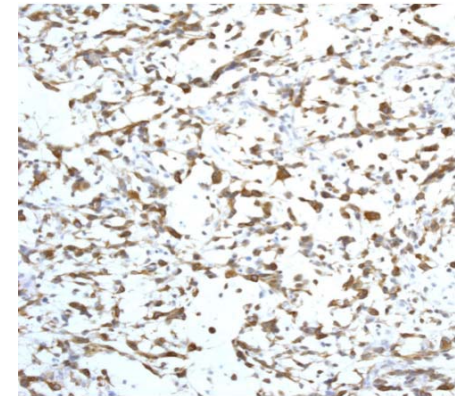




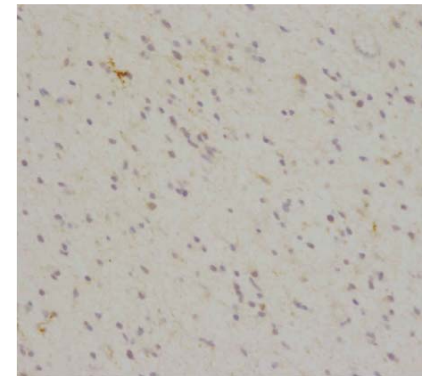
B



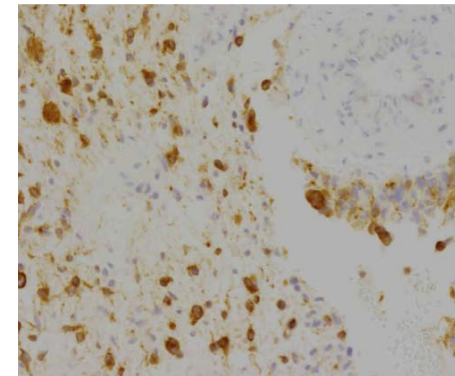
PDGFRA x20 Grade II



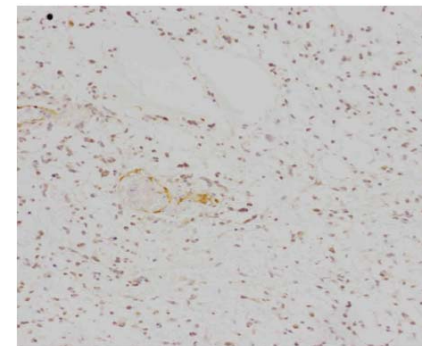
PDGFRA x20 Grade IV



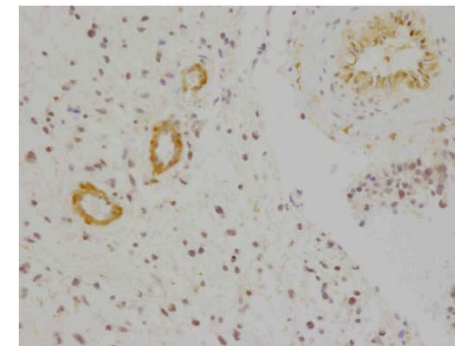
cKIT x20 Grade II



cKIT x20 Grade IV



PTEN x20 Grade II



PTEN x20 Grade IV